On the Single-Molecule Magnetic Behavior of Linear Iron(I) Arylsilylamides

Ruth Weller, Mihail Atanasov, Serhiy Demeshko, Ting-Yi Chen, Ivan Mohelsky, Eckhard Bill, Milan Orlita, Franc Meyer, Frank Neese, C. Gunnar Werncke

On the Single Molecule Magnetic Behavior of Linear Iron(I) Arylsilylamides

Ruth Weller,[‡] Mihail Atanasov,[#,¤] Serhiy Demeshko,[+] Ting-Yi Chen,[+] Ivan Mohelsky,[§] Eckhard Bill,[#] Milan Orlita,[§] Franc Meyer,[+] Frank Neese,[#] C. Gunnar Werncke[‡]

[‡]Department of Chemistry, Philipps-University Marburg, Hans-Meerwein-Straße 4, 35043 Marburg, Germany; [#]Max-Planck-Institut für Kohlenforschung, Kaiser-Wilhelm-Platz 1, 45470 Mülheim an der Ruhr, Germany; [¤] Institute of General and Inorganic Chemistry, Bulgarian Academy of Sciences, Akad.Georgi Bontchev Street, Bl.11, 1113 Sofia, Bulgaria; [+]Institute of Inorganic Chemistry, University of Göttingen, Tammannstr. 4, D-37077 Göttingen, Germany; [§]LAB National des Champs Magnétiques Intenses, LNCMI – CNRS, 25 Martyrs Avenue, BP 166, 38042 Grenoble Cedex 9, France

KEYWORDS Iron(I) silylamides, single molecule magnetism, Mössbauer spectroscopy, Computational analysis, Magneto infrared-spectroscopy

ABSTRACT: The rational design of 3d-metal based single-molecule magnets (SMM) requires a fundamental understanding of intrinsic electronic and structural properties and how they translate into experimentally observable features. Here, we determined the magnetic properties of the linear iron(I) silylamides K{crypt}[FeL_2] and [$KFeL_2$] (L = –N(Dipp)$SiMe_3$; crypt = 4,7,13,16,21,24-Hexaoxa-1,10-diazabicyclo[8.8.8]hexacosan). For the former, slow-relaxation of the magnetisation with a spin reversal barrier of U_{eff} = 152 cm^{-1} as well as a closed waist magnetic hysteresis and magnetic blocking below 2.5 K are observed. For the more linear [$KFeL_2$], in which the potassium cation is encapsulated by the aryl substituents of the amide ligands, the relaxation barrier and the blocking temperature increase to U_{eff} = 184 cm^{-1} and T_B = 4.5 K, respectively. The increase is rationalized by a more pronounced axial anisotropy in [$KFeL_2$] determined by dc-SQUID magnetometry. The effective relaxation barrier of [$KFeL_2$] is in agreement with the energy spacing between the ground and first excited magnetic state, as obtained by field-dependent IR-spectroscopy (178 cm^{-1}), magnetic measurements (208 cm^{-1}) as well as theoretical analysis (212 cm^{-1}). In comparison with literature, the results show that magnetic coercivity in linear iron(I) silylamides is driven by the degree of linearity in conjunction with steric encumbrance, whereas the ligand symmetry is a marginal factor.

Introduction

Single-molecule magnets (SMMs) have attained considerable interest as they pose potential for future applications in high-density information storage,[1] quantum computing,[2–5] and magnetic refrigeration.[6,7] SMMs are open-shell complexes displaying slow relaxation of the magnetisation that originates from the intrinsic properties of the molecular system.[8] When the complexes contain only one metal ion, they are also denoted as single-ion magnets (SIMs). The key feature is the presence of large magnetic anisotropy arising from partially filled, energetically degenerate orbitals. This can be prominently observed for trivalent lanthanide complexes, since 4f valence orbitals of Ln^{3+} are only little affected by the ligands, which allows for the coupling of non-zero orbital angular momentum with the total spin S. It gives rise to a total angular momentum J, and a potentially large magnetic anisotropy and has been exploited for a number of recent examples of lanthanide complexes that display large effective barriers for magnetisation reversal (U_{eff}) and high magnetic blocking temperatures (T_B).[9–11] In contrast, 3d-transition metal based SIMs face several disadvantages with regards to their lanthanide counterparts. They possess smaller magnetic moments and spin-orbit coupling constants. More importantly, strong interactions of the d-orbitals with the ligand field lead to quenching of first-order orbital contributions to the magnetic moment.[8] Recently, it has been shown that these disadvantages can in principal be overcome for 3d-metals in a linear ligand arrangement.[12–17] Here, the two-coordinated metal ion is capable to exhibit virtually unquenched orbital angular momentum due to the energetic indifference to Jahn-Teller distortions, the inherent weak ligand field and orbitally degenerated states.[18] In this regard, the seminal example constitutes the S = 3/2 system $[Fe(C(SiMe_3)_3)_2]^-$ with an effective relaxation barrier of U_{eff} = 226 cm^{-1} at zero field and the first-time observation of magnetic blocking for a mononuclear 3d-transition metal system (Figure 1, left).[12,19,20]

Figure 1. Linear iron(I) complexes with observable slow relaxation of the magnetization at low temperatures, with given relaxation barriers U_{eff} and calculated energy spacing between the magnetic ground state and the first excited state.[12–14]

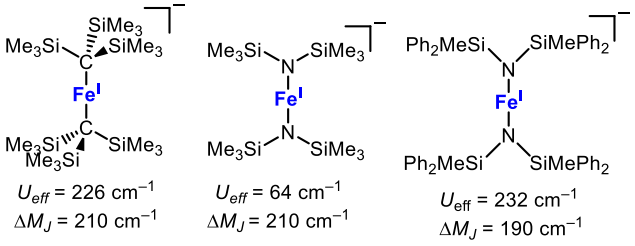

The value of the observable relaxation barrier is connected to the transition from M_J = ±7/2 ground state to the first excited M_J = ±5/2 state with a calculated energy separation of 210 cm^{-1}. More recently, this was amongst other expanded to the linear cobalt(II) complex (S = 3/2) [Co(CMe$_2$OR)$_2$] with a non-Aufbau L = 3 ground state and U_{eff} = 450 cm^{-1}.[13,14,21] The presence of an S = 3/2 ion in a (quasi)linear environment is thereby not a sufficient criterion for the observation of magnetic blocking behaviour.[15,22,23] For example, K{crypt}[Fe(N(SiMe$_3$)$_2$)$_2$] (Figure 1, middle, crypt = 4,7,13,16,21,24-Hexaoxa-1,10-diazabicyclo[8.8.8]-hexacosan) exhibited a barrier of magnetisation reversal in the absence of an applied dc-field of only U_{eff} = 64 cm^{-1},[15] although ab-initio ligand-field theory (AILFT) indicated similar properties as the for the seminal C_{3v}-symmetric [Fe(C(SiMe$_3$)$_3$)$_2$]$^-$.[24] This was originally attributed to the lower symmetry (C_{2V}) of the −N(SiMe$_3$)$_2$ ligand as well as its lower steric demand. Recently, however, it was shown by Murugesu and co-workers, that the bulky iron(I) silylamide K{crypt}[Fe(N(SiMePh$_2$)$_2$)$_2$] (Figure 1, right) exhibits a large spin reversal barrier of U_{eff} = 232 cm^{-1} and magnetic coercivity with closed-waist hysteresis up to 4 K.[21] It thus showed that the π-interactions of the nitrogen donor of the amide ligands as well as the local C_{2v} symmetry of the bis(silyl)amide ligands are no necessary detriments to substantial slow magnetic relaxation behaviour. In addition, computational analysis indicated that the orbital situation and orbital contributions to the magnetic moment are fairly robust towards moderate bending of the principal ligand axis (up to 40° for linear iron(I)).[21] Given the general synthetic flexibility of silyl amides and even more so of less symmetric arylsilylamides and derived linear metal complexes,[24–30] it was thus of interest to elucidate the magnetic properties of the seminal homoleptic iron(I) arylsilylamides [FeL$_2$]$^-$ (L = –N(Dipp)SiMe$_3$), Dipp = 2,6-diisopropylphenyl.

Herein, we present magnetic studies on iron(I) arylsilylamides, either as a salt, viz. a separated ion pair (K{crypt}**[FeL$_2$]**; L = –N(Dipp)SiMe$_3$), or with intramolecular potassium cation complexation (**[KFeL$_2$]**), revealing the impact of linearity of the ligand axis onto the magnetic relaxation. The behaviour of **[KFeL$_2$]** was subsequently understood by ab-initio ligand field analysis.

Results and Discussion

Synthesis and Structural Characterization

The prototypical example of a homoleptic iron(I) aryl/silylamide, [**FeL$_2$**]$^-$, is known for a few counter cations. Thereby, the anion can adopt different degrees of linearity (165° to 180°) as well as dihedral angles Si–N–N–Si (5° to 150°),[25,27,31,32] which depends on secondary interactions with the respective cation in solid state. Of these, only the K{18-crown-6} derivative K{18-crown-6}[**FeL$_2$**] was examined for its solid state magnetic properties,[27] however, with no mentioning or deliberate attempts for detection of single molecule magnetic behaviour. As such we contemplated using K{crypt}**[FeL$_2$]**,[31] that exhibits the most pronounced deviation from linearity (165.34(7)°). Here, the absence of volatile solvent molecules (either free in the crystal lattice or coordinated to the potassium cation) maintains the integrity of the crystalline solid upon isolation, and with it the crystallographically determined complex geometry. Secondly, **[K(dmap)$_2$FeL$_2$]** (dmap = N,N-dimethylaminopyridine) was a further prospective candidate, with a (crystallographically generated) perfect linear principal complex axis.[25,28] However, the presence of superparamagnetic impurities posed potential problems for unambiguous determination of its magnetic properties that, unfortunately, exacerbated upon multiple recrystallization processes. Thus, we fathomed the adduct free **[KFeL$_2$]**, which is known for the analogous nickel compound [KNiL$_2$].[28] **[KFeL$_2$]** was already obtained from KC$_8$ and [FeL$_2$], but only as a polymeric compound in solid state with the potassium ions linking neighbouring iron(I) amides *via* the aryl rings.[25] However, when the crystallization was now carried out from a saturated toluene solution at −40 °C (opposed to a *n*-pentane layered toluene solution in case of polymeric **[KFeL$_2$]$_\infty$**), consistently monomeric **[KFeL$_2$]** was obtained as dark red crystals (yield 88%, **Scheme 1**).

Scheme 1. Isolation of monomeric [KFe(N(Dipp)SiMe$_3$)$_2$] ([KFeL$_2$]).

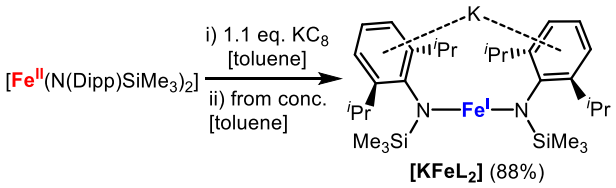

In solid state, **[KFeL$_2$]** shows a monomeric structure with the potassium ion encapsulated within the ligand sphere by the opposing aryl rings (**Figure 2**), akin to related iron, cobalt and nickel examples.[25,28] The Fe–N bond length is 1.914(3) Å, which is slightly longer than for K{crypt}**[FeL$_2$]**.[31] The Dipp-moieties are perfectly aligned with a dihedral angle of 0.3(3)°. The secondary potassium coordination further enforces a near linear N−Fe−N angle (177.79(18)°). Disregarding small deviations, the compound is overall C_{2v}-symmetric. In a toluene-d$_8$ solution the proton NMR spectrum of [**FeL$_2$**] matches that of the previously reported polymeric **[KFeL$_2$]$_\infty$**.[25] This implicates an identical speciation of both complexes in solution - namely in form of the monomeric **[KFeL$_2$]** - despite their difference concerning solid state structures with intra- and intermolecular potassium cation complexation.[25]

Figure 2. Solid state structure of [KFeL$_2$]. All hydrogen atoms are omitted for clarity. Selected bond lengths and angles: Fe−N 1.914(3) Å, K−Fe 3.5308(16) Å, K−Aryl 2.9290(5) Å, N−Fe−N' 177.79(18)°, Si–N–N'–Si' dihedral angle: 0.3(3)°.

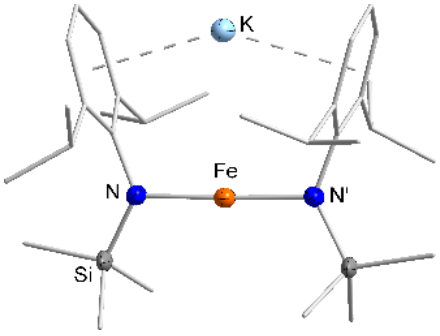

Figure 3. Zero-field ^{57}Fe Mössbauer spectrum of [KFeL$_2$] at 7 K. For parameters see Table 1.

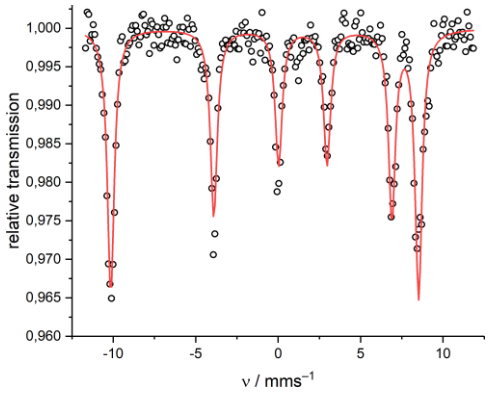

Table 1. Zero-field ^{57}Fe Mössbauer spectroscopic properties of mentioned linear iron(I) complexes.

Compound	δ (mm/s)	ΔE_Q (mm/s)	H_{int} (T)
K{crypt}[FeL$_2$]	0.34	−2.23	54.3
[K(dmap)$_2$FeL$_2$]	0.32	−2.30	60.1
[KFeL$_2$]	0.34	−2.31	58.0
K{crypt}[Fe(N(SiMe$_3$)$_2$)$_2$][15]	0.365	−2.37	55.85
K{crypt}[Fe(C(SiMe$_3$)$_3$)$_2$][12]	0.278	−2.52	63.97

Mössbauer spectroscopic and magnetic signatures

To gain insights into the electronic situation of [**KFeL$_2$**], [**K(dmap)$_2$FeL$_2$**] and **K{crypt}[FeL$_2$]**, their ^{57}Fe Mössbauer spectroscopic features were probed. At 80 K, no signal was observed in the ^{57}Fe Mössbauer spectrum for any compound. This phenomenon was already observed for the related iron(I) silylamide [Fe(N(SiMe$_3$)$_2$)$_2$]$^-$ and can be attributed to magnetic relaxation processes.[15] At 7 K, the spectra showed a sharp sextuplet for each compound with very similar isomer shifts, quadrupole splittings and internal magnetic fields. **K{crypt}[FeL$_2$],** for example, gave an isomer shift of δ = 0.34 mm/s, a quadrupole splitting of ΔE_Q = −2.23 mm/s and an internal field of H_{int} = 54.31 T. This aligns with the few other linear iron(I) complexes[12,15,18,33] and is indicative of single molecule magnetic behaviour. Most notably, the isomer shifts δ and quadrupol splittungs ΔE_Q of all [FeL$_2$]$^-$ complexes are slightly larger respectively smaller in comparison to that of the seminal [Fe(C(SiMe$_3$)$_3$)$_2$]$^-$, which reflects on the π-donating capabilities of the amide ligands.

Magnetic measurements of solid **[KFeL$_2$]** and **K{crypt}[FeL$_2$]** were performed between 2 and 210 K using a SQUID magnetometer (

Figure 4). Higher temperatures were not measured to prevent melting of the perfluorinated oil used for fixing the crystals and preventing their orientation in the magnetic field. At 200 K, the $\chi_M T$ value of **[KFeL$_2$]** is 3.63 cm^{3}Kmol^{-1} (

Figure 4A). Upon lowering the temperature, a slight increase to 3.65 cm^{3}Kmol^{-1} at 150 K was observed, which speaks to a degenerate ground state. The curve then steadily decreases to 3.13 cm^{3}Kmol^{-1} at 10 K, which is typical for transition metal complexes with contributions from first order angular momentum. A further sharp drop to 2.73 cm^{3}Kmol^{-1} at 2 K is detected. Together with variable temperature − variable field (VTVH) magnetisation measurements, the curves could be satisfactory modelled as a two-level system for an axial iron(I) with S = 3/2 (E/D = 0) using the spin Hamiltonian with Zeeman and zero field splitting $\hat{H} = \mu_B \vec{B} \boldsymbol{g} \vec{S} + D[\hat{S}_z^2 - \frac{1}{3}S(S+1) + {}^{E}/_{D}(\hat{S}_x^2 - \hat{S}_y^2)]$: This gave $g_x = g_y = 2.27$, $g_z = 3.31$ and $D = -104$ cm^{-1}. Although this ZFS formalism is formally forbidden for near-linear complexes with degenerate ground states[34] these values are in good congruence with those obtained from other methods (vide infra). For **K{crypt}[FeL$_2$]** the $\chi_M T$ vs T behaviour is similar with $\chi_M T$ = 3.95 cm^{3}Kmol^{-1} at 200 K (see ESI). Upon lowering the temperature, the value increases slightly to 3.97 cm^{3}Kmol^{-1} at 150 K, then steadily decreases to 3.48 cm^{3}Kmol^{-1} at 10 K with a further sharp drop to 3.05 cm^{3}Kmol^{-1} at 2 K. Together with VTVH magnetisation measurements (

Figure 4B) the curves could be satisfactory modelled using the abovementioned spin Hamiltonian to give g_x = 1.95, g_y = 2.61, g_z = 3.54, D = −92 cm^{-1} and E/D = 0.15. The values for **K{crypt}[FeL$_2$]** indicate a pronounced deviation from axial anisotropy in comparison to **[KFeL$_2$]** and point to the detrimental impact of the more bent geometry of the anion in **K{crypt}[FeL$_2$]** (165.34(7)°) compared to essentially linear **[KFeL$_2$]** (177.79(18)°), [Fe(N(SiMe$_3$)$_2$)$_2$]$^-$ (180°)[15] and [Fe(N(SiMePh$_2$)$_2$)$_2$]$^-$ (178.1°)[21]. As such, we were curious how this would translate to the dynamic magnetic relaxation behaviour of **[KFeL$_2$]** and **K{crypt}[FeL$_2$]**. Frequency dependent ac magnetic susceptibility measurements at various temperatures were performed to determine the relaxation barrier U_{eff}, for which an external magnetic field of 1000 Oe was used. The Arrhenius plot of the temperature dependence clearly deviated from the linear Arrhenius law, so additional relaxation processes were considered (direct, Raman, Orbach processes and quantum tunnelling of the magnetization (QTM)). For both complexes, the entire temperature range could be well fitted assuming Raman and Orbach relaxation pathways, using $\tau^{-1} = BT^n + \tau_0^{-1} \exp(-U_{eff}/k_B T)$. This gave a U_{eff} = 184 cm^{-1} for **[KFeL$_2$]** with $B = 3.8 \cdot 10^{-4}$ s^{-1}K^{-5}, n = 5, and $\tau_0 = 1.3 \cdot 10^{-9}$ s (

Figure 4C/D). **K{crypt}[KFeL$_2$]** showed a reduced relaxation barrier of U_{eff} = 152 cm^{-1} with $B = 6.3 \cdot 10^{-3}$ s^{-1}K^{-5}, n = 4.4, and $\tau_0 = 2.2 \cdot 10^{-9}$ s (see ESI). In comparison with the former it thus indicated that deviations from linearity are lowering the relaxation barriers due to a larger rhombicity of the magnetic anisotropy and pronounced QTM. To put these results into perspective, the relaxation barriers found for **[KFeL$_2$]** and **K{crypt}[FeL$_2$]** are in-between the values reported for K{crypt}[Fe(N(SiMe$_3$)$_2$)$_2$] (U_{eff} = 64 cm^{-1}),[15] as well as K{crypt}[Fe(N(SiMePh$_2$)$_2$)$_2$] (U_{eff} = 232 cm^{-1})[21] and K{crypt}[Fe(C(SiMe$_3$)$_3$)$_2$] (U_{eff} = 224 cm^{-1})[12].

Figure 4. ac/dc-Magnetic properties of [KFeL$_2$]. Solid lines depict fit according to the spin Hamiltonian using g_x = 2.27, g_y = 2.27, g_z = 3.31 and D = –104 cm^{-1} (E/D = 0). A) Temperature dependence of $\chi_M T$ at 5000 Oe between 2 and 210 K; B) VTVH magnetization measurements at 1, 4 and 7 T; C) Frequency dependence of χ'' at various temperatures (ΔT = 1 K) with an applied dc field of H_{dc} = 1000 Oe; D) Arrhenius-Plot of the temperature dependence of τ at H_{dc} = 1000 Oe; E) Magnetic hysteresis loop for various field sweep rates at 2.0 K; F) Zero-field-cooled/field-cooled (ZFC/FC) magnetization measurements.

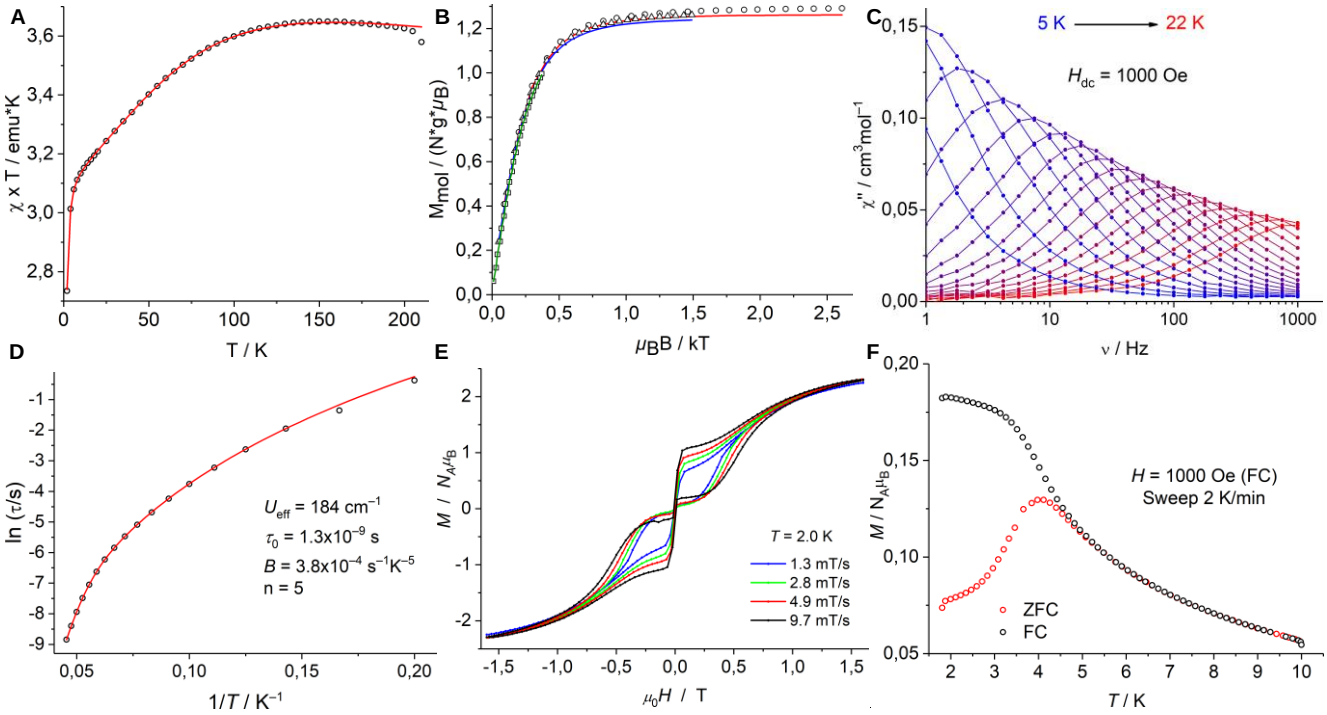

Especially the comparison with K{crypt}[Fe(N(SiMe$_3$)$_2$)$_2$] is informative as it underscores that strict linearity of a two-coordinate iron(I) anion is not a sufficient criterion for substantial slow magnetic relaxation behaviour – despite computational analyses indicated otherwise.[15] As such, steric congestion is of further importance as it likely mitigates vibrational distortions of the principal N–Fe–N axis as well as vibronic coupling. The difference with regards to K{crypt}[Fe(N(SiMe$_3$)$_2$)$_2$] is even more obvious in terms of magnetic coercivity as both, **[KFeL$_2$] (**

Figure 4E/F**)** and **K{crypt}[FeL$_2$]** (see ESI), show magnetic blocking and a closed-waist magnetic hysteresis. As indicated by the discontinuous steep decrease in $\chi_M T$ of **K{crypt}[FeL$_2$]** and **[KFeL$_2$]** at low-temperatures, a spin-reversal barrier becomes apparent upon cooling the samples with or without applied dc-field. For **K{crypt}[FeL$_2$],** deviations of the field-cooled (FC) and zero-field cooled (ZFC) measurements became apparent at 2 K but were not well-resolved (see ESI). Variable-field magnetisation data between 2.0 and 5.0 K showed hysteresis below 2.8 K for H ≠ 0 Oe. The hysteresis is waist-restricted, which is attributed to rapid relaxation processes *via* quantum tunnelling in the absence of any external field. For **[KFeL$_2$]**, the hysteresis is observed up to 4.5 K, in agreement with the blocking temperature (T_B = 4.5 K) obtained by ZFC/FC measurements (

Figure 4E/F). These observations align with those for K{crypt}[Fe(N(SiMePh$_2$)$_2$)$_2$][21] as well as K{crypt}[Fe(C(SiMe$_3$)$_3$)$_2$],[12] which suggests that the local symmetry of these anionic N/C-donor ligands as well as π-interactions are of no measurable significance for single molecule magnetic behaviour of a linear iron(I) complex.

Quantum chemical calculations

I. Ab Initio Ligand Field MO and Angular Overlap Model Analysis[35,36] of The Iron-Amido Bond in [KFeL$_2$]. For a better understanding of the electronic situation in **[KFeL$_2$]**, we turned to ab-initio ligand field analysis[37] (NEVPT2/CASSCF level), which has proven as a powerful tool for delineation of single-molecule magnetic features. Two-fold coordinated linear Fe(I) complexes with π-donor ligands possess a simple ligand-field MO diagram with one σ-antibonding d_{z2} and two π-antibonding $d_{xz,yz}$ and a non-bonding d_{xy},d_{x2-y2} orbital pair. The sp^2-hybridized nitrogen donor in linear silyl amides functions as π-donor toward iron with one Fe–N–C out-of-plane πy-orbital; the other in-plane orbital lobe πx is already engaged in two strong bonds to the silicon and carbon neighbours. Owing to the low-oxidation state of iron(I), its 4s orbital is low in energy and hybridizes with the $3d_{z2}$ orbital. This so-called $3d_{z2}$-4s mixing counteracts the σ antibonding effect and renders the nominally d_{z2}-orbital lowest in energy. Ab-initio ligand field theory allows to get the ligand field matrix, herein taken in a standard order of orbitals d_{xy}, d_{yz}, d_{z2}, d_{xz} and d_{x2-y2}, as given in Eq.1 (CASSCF/NEVPT2 results, in cm^{-1}). Diagonalization of this matrix leads to orbital energy eigenvalues (in cm^{-1}): 0, 3165,

3270, 3372, 6771, which are plotted in **Figure 5** along with contour plots including corresponding ligand orbital tails.

$$V_{AILFT} = \begin{bmatrix} -68 & 0 & 0 & -43 & 0 \\ 0 & 3454 & 14 & 0 & 62 \\ 0 & 14 & -2989 & 0 & 997 \\ -43 & 0 & 0 & -128 & 0 \\ 0 & 62 & 997 & 0 & -268 \end{bmatrix} \quad \text{(Eq.1)}$$

The topmost d_{yz}-MO reflects the out-of-plane π-antibonding effect due to the N-amido bond; the d_{xz} is expected to be almost non-bonding (*vide supra*). The d_{xy} and d_{x2-y2} orbitals have no ligand counterparts and are non-bonding. This is supported by the pseudo degeneracy of the second, third and fourth AILFT orbitals (3165, 3270, 3372 cm^{-1}, respectively). This bonding situation can be translated into a chemical language using the angular overlap model. For strictly linear arrangement (N–Fe–N bond angle 180°) this model yields the following expressions of the energy of the 3d-orbitals:

$$e(d_{dz2}) = 2(e_\sigma - e_{3d\,4s}) = 2e_\sigma^{eff}$$
$$e(d_{dyz}) = 2e_{\pi s} \quad \text{(Eqs. 2)}$$
$$e(d_{dxz}) = e(d_{xy}) = e(d_{x2-y2}) \approx 0$$

The parameter $e_{\pi s}$ quantifies the interaction between iron (I) d_{yz} and the out-of-plane π orbital of the amido donor ligand, the factor "2" accounts for the presence of two such donors. The parameter e_σ^{eff} is an effective one. Its value is governed by the N-σ antibonding energy, which would destabilize the d_{z2} orbital minus the energy connected with the $3d_{z2}$-4s mixing, which tends to stabilize this orbital. The computed energies in Eqs. 2 allow to estimate e_σ^{eff} and $e_{\pi s}$ to –1650 cm^{-1} and 1750 cm^{-1}, respectively. Thus, 3d-4s mixing dominates and renders the d_{z2} orbital lowest in energy (Figure 5).

Figure 5. d-Orbital splitting of [KFeL$_2$] from ab-initio ligand field analysis.

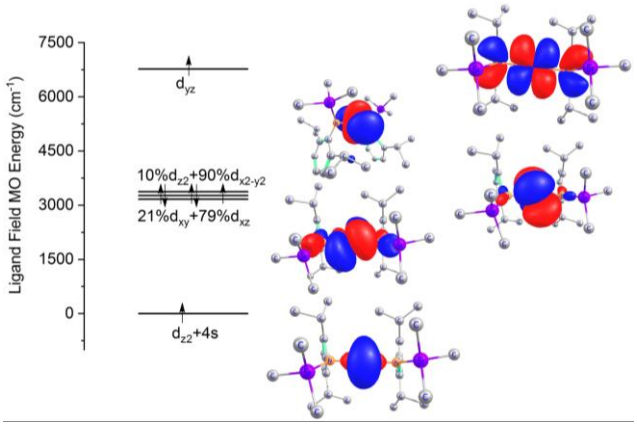

With seven d-electrons on the 3d-shell of iron(I) this results in a $(d_{z2}d_{xz}d_{x2y2}d_{xy})^6 d_{yz}^1$ ground state configuration. This ground state is expected to be a superposition of several different electron distributions. Calculations showed (see next section) that configurations $d_{z2}^1 d_{xz}^2 d_{z2-y2}^1 d_{xy}^2 d_{yz}^1$ and $d_{z2}^1 d_{xz}^1 d_{z2-y2}^2 d_{xy}^2 d_{yz}^1$ dominate (up to 97%) the pseudo-two fold degenerate ground state wave function. Here, the lowest-lying d_{z2} orbital is only singly occupied. It reflects on the weak ligand field, which is insufficient to overcome the electron-electron repulsions. The degeneracy is of great importance for the magnetic anisotropy and magnetic response which allow to qualify **[KFeL$_2$]** as a single molecule magnet.

II. Electronic structure and magnetic anisotropy of [KFeL$_2$] from CASSCF and CASSCF/NEVPT2 from ab-initio calculations. Twofold coordinate linear complexes of d^7 transition metal ions span two kind of spin-states – 10 S=3/2 and 40 S=1/2 spin-multiplets, from which the first give rise to two non-degenerate $^4\Sigma^-$ and four doubly degenerate $\pi^4\Pi(1)$, $^4\Pi(2)$, $^4\Delta$ and $^4\Phi$ many-particle states. Because of the π-anisotropy of the nitrogen donors of the two amido ligands, the doubly degenerate states split. In Table 2 we list their CASSCF energies, the compositions of the CASSCF wave functions and their NEVPT2 corrected energies. For the sake of transparency, only occupations of two β spin electrons in addition to the five singly occupied α spin 3d-MOs of the half-field shell are listed; d_{z2}, (d_{xz},d_{yz}) and (d_{x2-y2},d_{xy}) orbitals are designated by notations for the irreducible representations of the $C_{\infty v}$ point group. The ground state is of $^4\Delta$ symmetry and shows only tiny splitting due to the actual C_1 complex symmetry. This state is two-fold degenerate. Spin-orbit coupling induces orbital moments of $M_L = \pm 2$ which add to the $M_S = \pm 3/2$ spin-moments to a total angular momentum of $M_J = \pm 7/2$. It is remarkable that dynamical correlation (accounted for using NEVPT2) increases the gap between the ground $^4\Delta$ and the excited $^4\Pi(1)$ and $^4\Phi$ states spanning orbital moments of $M_L = \pm 1$ and $M_L = \pm 2$, respectively, by a factor of more than two. It is the small splitting of the well-defined, well separated $^4\Delta$ ground state which renders all these kind of complexes not sensitive to the nature of the linear donor (nitrogen or carbon) and less, but still sensitive to deviations from the linear geometry (as the comparison between **[KFeL$_2$]** and **K{crypt}[FeL$_2$]** clearly shows).

Table 2. Energies of the *S* = 3/2 spin state manifold from CASSCF and NEVPT2 scalar relativistic calculations along with compositions (in %) of the CASSCF wave functions.[a]

State	CASSCF		NEVPT2
	Energy (cm^{-1})	Composition	Energy (cm^{-1})
x	0	100 $\sigma\delta$	156
	14	100 $\sigma\delta$	0
$^4\Pi(1)$	3288	50 $\sigma\pi$ + 47 $\pi\delta$	7827
	3491	31 $\sigma\pi$ + 67 $\pi\delta$	9368
$^4\Phi$	4688	83 $\pi\delta$ +17 $\sigma\pi$	11238
	5047	84 $\pi\delta$ +19 $\sigma\pi$	11901
$^4\Sigma^-$	6385	60 π^2 + 37 δ^2	13797
$^4\Pi(2)$	15688	67 $\pi\delta$ + 33 $\sigma\pi$	18307
	18912	50 $\pi\delta$ + 49 $\sigma\pi$	21468
$^4\Sigma^-$	19246	39 π^2 + 61 δ^2	22862

[a] Listed are occupations of β spin-orbitals on top of the α spin half-filled shell of iron(I).

Table 3. Spin-orbit splitting of the $^4\Delta$ ground state of [KFeL$_2$] and g-factors for the ground and the three excited Kramer's doublets (KD1-4) computed using CASSCF wave functions and diagonal corrections to the energy from NEVPT2.

	CASSCF				NEVPT2			
	E / cm^{-1}	g_1	g_2	g_3	E / cm^{-1}	g_1	g_2	g_3
KD1	0	0.002	0.002	9.961	0	0.018	0.018	9.876
KD2	210	0.276	0.279	5.963	212	2.271	2.272	5.321
KD3	447	0.056	0.472	1.967	497	1.318	2.153	2.386
KD4	707	0.142	0.154	2.032	733	0.085	0.086	2.135

Under the effect of spin-orbit coupling, the $^4\Delta$ ground state splits into four Kramer's doublets whose CASSCF and NEVPT2 energies and effective g-factors are listed in Table 3. The aforementioned M_J = ±7/2 character of the ground state renders the ground state Kramer's doublet purely anisotropic with negligibly small hard axes g-factor values (0.002) and large easy axis value (9.961, close to the atomic limit of g = 10). In contrast, g-factors for the first excited state are less anisotropic (CASSCF: 0.276, 0.279 and 5.963; NEVPT2: 2.271, 2.272, 5.321). As discussed in the text, this is of importance for the magnetic anisotropy. It is finally instructive to compare **[KFeL$_2$]** with the cobalt(II) dialkyl complex [Co(C(SiMe$_2$ONaph)$_3$)$_2$] with Co in the same d^7 configuration but in a higher oxidation state.[13] The oxidation state increase by one leads to a weakening of the 3d$_{z2}$-4s mixing rendering, now d$_{z2}$ topmost in energy. The relatively weaker (compared to **[KFeL$_2$]**) destabilization of the d$_{xz}$, d$_{yz}$ orbital pair (due to engagement of the carbon 2p$_x$,2p$_y$ orbitals in bonds to silicon) leads to narrowing of this orbital pair to the non-bonding d$_{x2-y2}$,d$_{xy}$ orbitals; a non-Hund (d$_{x2-y2}$,d$_{xy}$)^3(d$_{yz}$,d$_{xz}$)^{3}d$_{z2}^1$ ground state with orbital contributions of M_L = ±3 to the M_S = ±3/2 electron spin results. The M_J = ±7/2 ground state sets a top limit of magnetic anisotropy achievable in transition metal complexes. Looking at the orbital splitting (Figure 5), it gives an orbital ordering of d$_{z²}$+4s, nearly degenerate d$_{xy}$, d$_{xz}$ and d$_{x²-y²}$ orbitals and a highest lying d$_{yz}$. This is similar to the one of the more symmetric [Fe(N(SiMe$_3$)$_2$)$_2$]$^-$,[15] showing a marginal impact of the herein used aryl/silylamide. The ^{4}E ground state splits into four doublets, which are best characterised by the magnetic quantum number M_J (J = total angular momentum). The four doublets would then correspond to M_J = ±7/2, ±5/2, ±3/2 and ±1/2, with an energy spacing between the lowest doublets (M_J = ±7/2, ±5/2) of 212 cm^{-1}. The energy spacing is in excellent agreement with the value obtained from the temperature dependent susceptibility data (2D = 208 cm^{-1}). The M_J = ±7/2 ground state is highly anisotropic (g$_x$ = g$_y$ = 0.018, g$_z$ = 9.876). The less axial, anisotropic first excited magnetic state M_J = ±5/2 (g$_x$ = g$_y$ = 2.271, g$_z$ = 5.321) indicates that the magnetic relaxation in **[KFeL$_2$]** likely occurs *via* thermally assisted through-barrier tunnelling of the excited state.

Direct determination of the energy spacing between ground and first excited magnetic state.

For confirmation of the experimentally and computationally determined energy spacing between the ground and first excited M_J state, we turned to field-dependent IR spectroscopy of the far-red region. This is of special importance as the common determination of D *via* the magnetisation data is subject to the limits of the fitting procedure for quasilinear complexes and further provides only an indirect measure for the excitation from the ground to the excited state. Magneto-transmission spectra on **[KFeL$_2$]** were recorded in the spectral range 100 – 400 cm^{-1}, at 4.2 K and in an applied field B ranging from 0 to 16 T (in steps of 1 T). A field dependent absorption band was detected at 178 cm^{-1}.

Figure 6. Stacked far-IR magneto-transmission (T_B) spectra of complex [KFeL$_2$] at 4.2 K in an applied magnetic field (B = 1-16 T), normalized to the zero-field transmission T_0. The observed response indicates a single absorption mode which shifts towards higher energies with the applied magnetic field (total shift of 14 cm^{-1} at 16 T).

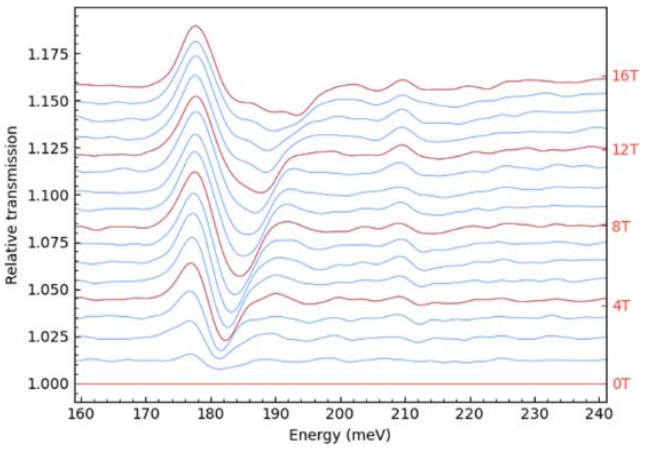

The obtained value is in the range of the computed (212 cm^{-1}) and experimentally determined (2D = 208 cm^{-1}) energy spacing between the ground and the first excited magnetic state. Increasing the field to 16 T leads to a blue shift of 14 cm^{-1} that perfectly matches the expected value of 15 cm^{-1}, which arises from different field dependencies of the energies of the involved states.

CONCLUSION

Overall, we present a comprehensive analysis of the single-molecule magnetic behaviour of two-coordinate iron(I) complexes **K{crypt}[FeL$_2$]** and **[KFeL$_2$]** (L = –

N(Dipp)SiMe$_3$). The quasilinear **[KFeL$_2$]**, for which linearity is enforced by intramolecular potassium complexation, shows a closed-waist hysteresis and magnetic blocking up to 4.5 K as well as a barrier for slow relaxation of magnetisation of U_{eff} = 184 cm^{-1}. Using ab-initio ligand field analysis as well as magneto-IR-spectroscopy, the relaxation behaviour could be rationalized as an excitation from the magnetic ground state (M_J = ±7/2) to the first excited state (M_J = ±5/2). Due to the computed pronounced rhombicity of the excited state this is likely followed by through-barrier tunnelling. The less linear separated ion pair complex **K{crypt}[FeL$_2$]** shows a reduced magnetic coercivity, which can be attributed to a non-negligible magnetic rhombicity of the ground state. In light of literature precedence, it can be concluded that pronounced single-ion magnetic features in case of two-coordinate iron(I) relies primarily on a (near-)linear principal axis in conjunction with sterically encumbered ligands, to possibly reduce vibrational motions. The local symmetry of the used anionic donor ligand and the presence of π-interactions is apparently a less relevant factor. This study thus conceptionally expands the synthetic possibilities for mononuclear transition metal complexes that show magnetic blocking, and it might be applicable to other quasilinear ligand architectures.

EXPERIMENTAL SECTION

All manipulations were carried out in a glovebox under a dry argon atmosphere, unless indicated otherwise. Used solvents were dried by continuous distillation over sodium metal for several days. Deuterated solvents were used as received, degassed *via* three freeze-pump cycles and stored over molecular sieves (4 Å). The ^{1}H NMR spectra were recorded on a Bruker AV 500, a Bruker HD 500 or a Bruker HD 300 NMR spectrometer (Bruker Corporation, Billerica, USA). Chemical shifts are reported in ppm relative to the residual proton signals of the solvent (for ^{1}H). $w_{1/2}$ is the line width of a signal at half its maximum intensity. Integrals of the broad signals ligand set were obtained directly or by peak fitting (in case of overlapping signals) using the MestreNova software package (Mestrelab, Santiago de Compostela, Spain). Elemental analysis were performed by the "in-house" service of the Chemistry Department of the Philipps University Marburg, Germany using a CHN(S) analyzer vario MICRO Cube (Elementar Analysensysteme GmbH, Langenselbold, Germany). K{crypt}[Fe(N(Dipp)SiMe$_3$)$_2$][31] and [Fe(N(Dipp)SiMe$_3$)$_2$][38] were prepared according to literature procedures.

[KFe(N(Dipp)SiMe$_3$)$_2$] ([KFeL$_2$]): One equivalent of [Fe(N(Dipp)SiMe$_3$)$_2$] (200 mg, 0.36 mmol) was dissolved in 5 mL toluene. After adding KC_8 (0.40 mmol, 1.1 equiv.) the reaction mixture was stirred for several minutes at room temperature, while a change in color to red was observed. The graphite was filtered off and all volatiles were evaporated off. Crystals, suitable for x-ray diffraction analysis, were obtained from a saturated solution of **[KFeL$_2$]** in toluene at −40 °C. [25] **Yield:** 187 mg (0.32 mmol, 88%). ^{1}H NMR spectroscopic data in toluene-d$_8$ and combustion analysis matches that of polymeric form **[KFeL$_2$]$_\infty$**[25]. **IR** (ATR, cm^{-1}): $\tilde{\nu}$ = 3051 (w), 2948 (m), 2885 (w), 2864 (m), 1576 (w), 1458 (m), 1417 (s), 1378 (m), 1357 (m), 1316 (m), 1238 (s), 1197 (m), 1155 (w), 1141 (w), 1101 (m), 1052 (m), 1040 (m), 936 (m), 915 (s), 878 (m), 827 (vs), 787 (s), 746 (m), 671 (m), 627 (m), 579 (w), 535 (m), 422 (m).

X-Ray Diffraction Analysis

Data for compound [KFe(N(Dipp)SiMe$_3$)$_2$] (**[KFeL$_2$]**) (CCDC 2113327) were collected on a STOE IPDS2 diffractometer (STOE & Cie GmbH, Darmstadt, Germany) using a graphite-monochromated Mo-Kα radiation (λ = 0.71073 Å), equipped with an Oxford Instrument Cooler Device (Oxford Instruments, Abingdon, UK). The structure has been solved using either OLEX SHELXT V2014/1[39] and refined by means of least-squares procedures on an F^2 with the aid of the program SHELXL-2016/6[40] included in the software package WinGX version 1.63[41] or using CRYSTALS[42]. The atomic scattering factors were taken from International Tables for X-ray Crystallography.[43] All non-hydrogen atoms were refined anisotropically. All hydrogen atoms were refined by using a riding model. Disorders were found in the trimethylsilyl moiety and were modelled accordingly. The absorption correction was introduced by using the MULTISCAN and X-Red programs.[44,45] The drawing of the molecule is performed with the program DIAMOND (Crystal Impact, Bonn, Germany) with 50% probability displacement ellipsoids for non-H atoms.

^{57}Fe Mössbauer spectroscopy

The Mössbauer spectrum was recorded with a ^{57}Co source in a Rh matrix using an alternating constant acceleration *Wissel* Mössbauer spectrometer operated in the transmission mode and equipped with a *Janis* closed-cycle helium cryostat. Isomer shifts are given relative to iron metal at ambient temperature. Simulation of the experimental data was performed with the *MF* program using *Lorentzian* line sextets: E. Bill, Max-Planck Institute for Chemical Energy Conversion, Mülheim/Ruhr, Germany.

Magnetic Measurements

Temperature-dependent magnetic susceptibility measurements were carried out with a *Quantum-Design* MPMS3 SQUID magnetometer equipped with a 7 Tesla magnet in the range from 2 to 210 K in a magnetic field of 0.5 T. The polycrystalline sample was contained in a polycarbonate capsule, covered with a few drops of low viscosity perfluoropolyether based inert oil Fomblin Y45 to fix the crystals, and fixed in a non-magnetic sample holder. The maximum measuring temperature of 210 K was chosen because of the pour point of the oil, in order to keep the oil in the frozen state and to avoid therefore the orientation of the crystals parallel to the magnetic field. Each raw data file for the measured magnetic moment was corrected for the diamagnetic contribution of the capsule and of the inert oil according to $M^{dia} = \chi_g mH$, with experimentally obtained gram susceptibility of the capsule ($\chi_g = -5.60 \cdot 10^{-7}$ emu/(g·Oe) and of the oil ($\chi_g = -3.82 \cdot 10^{-7}$ emu/(g·Oe)). The molar susceptibility data were corrected for the diamagnetic contribution according to χ_M^{dia}(sample) = $-0.5 \cdot M\ 10^{-6}$ cm^3 mol^{-1}.[46] Experimental $\chi_M T$ vs. T data were modelled using a fitting procedure to the following spin Hamiltonian for one iron(I) ion (S = 3/2) with Zeeman splitting and zero-field splitting:

$$\hat{H} = \mu_B \vec{B} \boldsymbol{g} \vec{S} + D[\hat{S}_z^2 - \frac{1}{3}S(S+1) + {}^{E}/_{D}\,(\hat{S}_x^2 - \hat{S}_y^2)].$$

Full-matrix diagonalization of the spin Hamiltonian was performed with the julX_2s program (E. Bill, Max-Planck Institute for Chemical Energy Conversion, Mülheim/Ruhr, Germany, 2014). Matrix diagonalization is done with the routine ZHEEV from the LAPACK numerical package. Parameter optimization is performed with the simplex routine AMOEBA from NUMERICAL RECIPES.

MAGNETO INFRARED SPECTROSCOPY

To enable infrared experiments in the transmission configuration, the studied compounds were first mixed with eicosane in the approximate ratio of 1:20 and a pressed pellet was prepared. The sample was placed in a superconducting and kept at T= 4.2 K in the

exchange helium. Then, the THz/infrared radiation from a globar was analyzed by a Vertex 80v FTIR spectrometer, delivered using light-pipe optics to the pellet and detected using a composite bolometer placed just below the pellet. The measured transmission spectra are presented in a form of relative magneto-transmission, T_B/T_0, to emphasize the field-induced spectral features.

QUANTUM CHEMICAL CALCULATIONS

Electronic energies and wave functions of electronic multiplets of [**KFeL$_2$**] were computed using the Complete Active Space Self-Consistent Field (CASSCF) method[47] along with a minimal active space of seven electrons in the five metal d-based molecular orbitals. The CASSCF method leads in general to superposition of configurations. Herein, spin-eigenfunctions (Configuration State Functions, CSF) are taken as a many particle basis. This method accounts for static (left-right) electron correlation. The CASSCF wave functions provide model-space (zeroth-order function) for a more rigorous treatment, in which dynamic electron correlation is taken into account. The way this is usually done is using second order perturbation theory. In this work we employed the N-Electron Valence Perturbation Theory to second order method (NEVPT2).[48–50] Spin-orbit coupling (SOC) leads to splitting of the scalar relativistic (spin-free) states into Kramer's doublets (known as zero-field splitting, ZFS) and application of a magnetic field leads to further splitting of each Kramers doublet into spin-sublevels due to the Zeeman effect. SOC and the Zeeman effect lead to violation of the spin-symmetry. In our calculations SOC and magnetic field effects are taken into account using quasi-deregenerate perturbation theory (QDPT) in the basis of the CASSCF eigenfunctions.[51,52]

ASSOCIATED CONTENT

Supporting Information: IR/Raman spectra of **[KFeL$_2$]**. Further magnetic and /^{57}Fe Mössbauer spectroscopic data for K{crypt}**[FeL$_2$]**, **[KFeL$_2$] and [K(dmap)$_2$FeL$_2$]**. Additional computational details for **[KFeL$_2$]**. This material is available free of charge via the Internet at "http://pubs.acs.org."

AUTHOR INFORMATION

Corresponding Author

* E-Mail: gunnar.werncke@chemie.uni-marburg.de.

Author Contributions

The manuscript was written through contributions of all authors. All authors have given approval to the final version of the manuscript.

Funding Sources

We thank the Deutsche Forschungsgemeinschaft (DFG, German Research Foundation) for support by personal grants (WE 5627/4-1 and WE 5627/4-2 for C. G. W.) as well as in the framework of the Research Training Group BENCh (RTG 2455, project 389479699). Purchase of the SQUID magnetometer was supported by the DFG (project number INST 186/1329-1 FUGG) and the Niedersächsische Ministerium für Wissenschaft und Kultur (MWK).

REFERENCES

(1) Mannini, M.; Pineider, F.; Sainctavit, P.; Danieli, C.; Otero, E.; Sciancalepore, C.; Talarico, A. M.; Arrio, M.-A.; Cornia, A.; Gatteschi, D.; Sessoli, R. Magnetic memory of a single-molecule quantum magnet wired to a gold surface. *Nat. Mater.* **2009**, *8* (3), 194–197. DOI: 10.1038/nmat2374.

(2) Stamp, P. C. E.; Gaita-Ariño, A. Spin-based quantum computers made by chemistry: hows and whys. *J. Mater. Chem.* **2009**, *19* (12), 1718–1730. DOI: 10.1039/B811778K.

(3) Ardavan, A.; Rival, O.; Morton, J. J. L.; Blundell, S. J.; Tyryshkin, A. M.; Timco, G. A.; Winpenny, R. E. P. Will spin-relaxation times in molecular magnets permit quantum information processing? *Phys. Rev. Lett.* **2007**, *98* (5), 57201. DOI: 10.1103/PhysRevLett.98.057201.

(4) Leuenberger, M. N.; Loss, D. Quantum computing in molecular magnets. *Nature* **2001**, *410* (6830), 789–793. DOI: 10.1038/35071024.

(5) Moreno-Pineda, E.; Wernsdorfer, W. Measuring molecular magnets for quantum technologies. *Nat Rev Phys* **2021**, *3* (9), 645–659. DOI: 10.1038/s42254-021-00340-3.

(6) Torres, F.; Hernández, J. M.; Bohigas, X.; Tejada, J. Giant and time-dependent magnetocaloric effect in high-spin molecular magnets. *Appl. Phys. Lett.* **2000**, *77* (20), 3248–3250. DOI: 10.1063/1.1325393.

(7) Zheng, Y.-Z.; Zhou, G.-J.; Zheng, Z.; Winpenny, R. E. P. Molecule-based magnetic coolers. *Chem. Soc. Rev.* **2014**, *43* (5), 1462–1475. DOI: 10.1039/C3CS60337G.

(8) Frost, J. M.; Harriman, K. L. M.; Murugesu, M. The rise of 3-d single-ion magnets in molecular magnetism:Towards materials from molecules? *Chem. Sci.* **2016**, *7* (4), 2470–2491. DOI: 10.1039/C5SC03224E.

(9) Guo, F.-S.; Day, B. M.; Chen, Y.-C.; Tong, M.-L.; Mansikkamäki, A.; Layfield, R. A. A Dysprosium Metallocene Single-Molecule Magnet Functioning at the Axial Limit. *Angew. Chem. Int. Ed.* **2017**, *56* (38), 11445–11449. DOI: 10.1002/anie.201705426.

(10) Goodwin, C. A. P.; Ortu, F.; Reta, D.; Chilton, N. F.; Mills, D. P. Molecular magnetic hysteresis at 60 kelvin in dysprosocenium. *Nature* **2017**, *548* (7668), 439–442. DOI: 10.1038/nature23447.

(11) Guo, F.-S.; Day, B. M.; Chen, Y.-C.; Tong, M.-L.; Mansikkamäki, A.; Layfield, R. A. Magnetic hysteresis up to 80 kelvin in a dysprosium metallocene single-molecule magnet. *Science* **2018**, *362* (6421), 1400–1403. DOI: 10.1126/science.aav0652.

(12) Zadrozny, J. M.; Xiao, D. J.; Atanasov, M.; Long, G. J.; Grandjean, F.; Neese, F.; Long, J. R. Magnetic blocking in a linear iron(I) complex. *Nat. Chem.* **2013**, *5* (7), 577–581. DOI: 10.1038/nchem.1630.

(13) Bunting, P. C.; Atanasov, M.; Damgaard-Møller, E.; Perfetti, M.; Crassee, I.; Orlita, M.; Overgaard, J.; van Slageren, J.; Neese, F.; Long, J. R. A linear cobalt(II) complex with maximal orbital angular momentum from a non-Aufbau ground state. *Science* **2018**, *362* (6421). DOI: 10.1126/science.aat7319.

(14) Yao, X.-N.; Du, J.-Z.; Zhang, Y.-Q.; Leng, X.-B.; Yang, M.-W.; Jiang, S.-D.; Wang, Z.-X.; Ouyang, Z.-W.; Deng, L.; Wang, B.-W.; Gao, S. Two-Coordinate Co(II) Imido Complexes as Outstanding Single-Molecule Magnets. *J. Am. Chem. Soc.* **2017**, *139* (1), 373–380. DOI: 10.1021/jacs.6b11043.

(15) Werncke, C. G.; Bunting, P. C.; Duhayon, C.; Long, J. R.; Bontemps, S.; Sabo-Etienne, S. Two-coordinate iron(I) complex [Fe{N(SiMe3)2}2](-) Synthesis, properties, and redox activity. *Angew. Chem. Int. Ed.* **2015**, *54* (1), 245–248. DOI: 10.1002/anie.201408802.

(16) Alexander Merrill, W.; Stich, T. A.; Brynda, M.; Yeagle, G. J.; Fettinger, J. C.; Hont, R. D.; Reiff, W. M.; Schulz, C. E.; Britt, R. D.; Power, P. P. Direct Spectroscopic Observation of Large Quenching of First-Order Orbital Angular Momentum with Bending in Monomeric, Two-Coordinate Fe(II) Primary Amido Complexes and the Profound Magnetic Effects of the Absence of Jahn− and Renner−Teller Distortions in Rigorously Linear Coordination. *J. Am. Chem. Soc.* **2009**, *131* (35), 12693–12702. DOI: 10.1021/ja903439t.

(17) Bryan, A. M.; Lin, C.-Y.; Sorai, M.; Miyazaki, Y.; Hoyt, H. M.; Hablutzel, A.; LaPointe, A.; Reiff, W. M.; Power, P. P.; Schulz, C. E. Measurement of extreme hyperfine fields in two-coordinate high-spin Fe2+ complexes by Mossbauer spectroscopy: essentially free-ion magnetism in the solid state. *Inorg. Chem.* **2014**, *53* (22), 12100–12107. DOI: 10.1021/ic501925e.

(18) Reiff, W. M.; LaPointe, A. M.; Witten, E. H. Virtual Free Ion Magnetism and the Absence of Jahn−Teller Distortion in a Linear Two-Coordinate Complex of High-Spin Iron(II). *J. Am. Chem. Soc.* **2004**, *126* (33), 10206–10207. DOI: 10.1021/ja030632w.

(19) Zadrozny, J. M.; Xiao, D. J.; Long, J. R.; Atanasov, M.; Neese, F.; Grandjean, F.; Long, G. J. Mössbauer spectroscopy as a probe of

magnetization dynamics in the linear iron(I) and iron(II) complexes Fe(C(SiMe3)3)2(1-/0.). *Inorg. Chem.* **2013**, *52* (22), 13123–13131. DOI: 10.1021/ic402013n.

(20) Thomsen, M. K.; Nyvang, A.; Walsh, J. P. S.; Bunting, P. C.; Long, J. R.; Neese, F.; Atanasov, M.; Genoni, A.; Overgaard, J. Insights into Single-Molecule-Magnet Behavior from the Experimental Electron Density of Linear Two-Coordinate Iron Complexes. *Inorg. Chem.* **2019**, *58* (5), 3211–3218. DOI: 10.1021/acs.inorgchem.8b03301.

(21) Errulat, D.; Harriman, K. L. M.; Gálico, D. A.; Ovens, J. S.; Mansikkamäki, A.; Murugesu, M. Aufbau vs. non-Aufbau ground states in two-coordinate d 7 single-molecule magnets. *Inorg. Chem. Front.* **2021**, *8* (23), 5076–5085. DOI: 10.1039/D1QI00912E.

(22) Samuel, P. P.; Mondal, K. C.; Amin Sk, N.; Roesky, H. W.; Carl, E.; Neufeld, R.; Stalke, D.; Demeshko, S.; Meyer, F.; Ungur, L.; Chibotaru, L. F.; Christian, J.; Ramachandran, V.; van Tol, J.; Dalal, N. S. Electronic Structure and Slow Magnetic Relaxation of Low-Coordinate Cyclic Alkyl(amino) Carbene Stabilized Iron(I) Complexes. *J. Am. Chem. Soc.* **2014**, *136* (34), 11964–11971. DOI: 10.1021/ja5043116.

(23) Chakraborty, U.; Demeshko, S.; Meyer, F.; Rebreyend, C.; Bruin, B. de; Atanasov, M.; Neese, F.; Mühldorf, B.; Wolf, R. Electronic Structure and Magnetic Anisotropy of an Unsaturated Cyclopentadienyl Iron(I) Complex with 15 Valence Electrons. *Angew. Chem. Int. Ed.* **2017**, *56* (27), 7995–7999. DOI: 10.1002/anie.201702454.

(24) Werncke, C. G.; Suturina, E.; Bunting, P. C.; Vendier, L.; Long, J. R.; Atanasov, M.; Neese, F.; Sabo-Etienne, S.; Bontemps, S. Homoleptic Two-Coordinate Silylamido Complexes of Chromium(I), Manganese(I), and Cobalt(I). *Chem. Eur. J.* **2016**, *22* (5), 1668–1674. DOI: 10.1002/chem.201503980.

(25) Weller, R.; Müller, I.; Duhayon, C.; Sabo-Etienne, S.; Bontemps, S.; Werncke, C. G. Quasilinear 3d-metal(i) complexes [KM(N(Dipp)SiR 3) 2] (M = Cr–Co) – structural diversity, solution state behaviour and reactivity. *Dalton Trans.* **2021**, *50*, 4890–4903. DOI: 10.1039/D1DT00121C.

(26) Weller, R.; Ruppach, L.; Shlyaykher, A.; Tambornino, F.; Werncke, C. G. Homoleptic quasilinear metal(i/ii) silylamides of Cr-Co with phenyl and allyl functions - impact of the oxidation state on secondary ligand interactions. *Dalton Trans.* **2021**, *50* (31), 10947–10963. DOI: 10.1039/D1DT01543E.

(27) Lin, C.-Y.; Fettinger, J. C.; Grandjean, F.; Long, G. J.; Power, P. P. Synthesis, Structure, and Magnetic and Electrochemical Properties of Quasi-Linear and Linear Iron(I), Cobalt(I), and Nickel(I) Amido Complexes // Synthesis, structure, and magnetic and electrochemical properties of quasi-linear and linear iron(I), cobalt(I), and nickel(I) amido complexes. *Inorg. Chem.* **2014**, *53* (17), 9400–9406. DOI: 10.1021/ic501534f.

(28) Lipschutz, M. I.; Yang, X.; Chatterjee, R.; Tilley, T. D. A Structurally Rigid Bis(amido) Ligand Framework in Low-Coordinate Ni(I), Ni(II), and Ni(III) Analogues Provides Access to a Ni(III) Methyl Complex via Oxidative Addition. *J. Am. Chem. Soc.* **2013**, *135* (41), 15298–15301. DOI: 10.1021/ja408151h.

(29) Lipschutz, M. I.; Tilley, T. D. Synthesis and reactivity of a conveniently prepared two-coordinate bis(amido) nickel(II) complex. *Chem. Commun.* **2012**, *48* (57), 7146–7148. DOI: 10.1039/c2cc32974c.

(30) Cai, I. C.; Lipschutz, M. I.; Tilley, T. D. A bis(amido) ligand set that supports two-coordinate chromium in the +1, +2, and +3 oxidation states. *Chem. Commun.* **2014**, *50* (86), 13062–13065. DOI: 10.1039/C4CC06615D.

(31) Reith, S.; Demeshko, S.; Battistella, B.; Reckziegel, A.; Schneider, C.; Stoy, A.; Lichtenberg, C.; Meyer, F.; Munz, D.; Werncke, C. G. Between imide, imidyl and nitrene - an imido iron complex in two oxidation states. *Chem. Sci.* **2022**, *13* (26), 7907–7913. DOI: 10.1039/D2SC01088G.

(32) Weller, R.; Völlinger, L.; Werncke, C. G. On the Synthesis and Reduction of Trigonal Halido Bis(silylamido) Metalates of Chromium to Cobalt. *Eur. J. Inorg. Chem.* **2021**, *2021* (42), 4383–4392. DOI: 10.1002/ejic.202100716.

(33) Reiff, W. M.; Schulz, C. E.; Whangbo, M.-H.; Seo, J. I.; Lee, Y. S.; Potratz, G. R.; Spicer, C. W.; Girolami, G. S. Consequences of a Linear Two-Coordinate Geometry for the Orbital Magnetism and Jahn−Teller Distortion Behavior of the High Spin Iron(II) Complex Fe[N(t -Bu) 2] 2. *J. Am. Chem. Soc.* **2009**, *131* (2), 404–405. DOI: 10.1021/ja806660f.

(34) Maurice, R.; Broer, R.; Guihéry, N.; Graaf, C. de. Zero-Field Splitting in Transition Metal Complexes: Ab Initio Calculations, Effective Hamiltonians, Model Hamiltonians, and Crystal-Field Models. In *Handbook of relativistic quantum chemistry*; Liu, W., Ed.; Springer reference; Springer, 2017; pp 765–796. DOI: 10.1007/978-3-642-40766-6_37.

(35) Schäffer, C. E.; Jørgensen, C. K. The angular overlap model, an attempt to revive the ligand field approaches. *Molecular Physics* **1965**, *9* (5), 401–412. DOI: 10.1080/00268976500100551.

(36) Schäffer, C. E. A perturbation representation of weak covalent bonding. *Structure and Bonding* **1968**, *5*, 68–95.

(37) Atanasov, M.; Ganyushin, D.; Sivalingam, K.; Neese, F. A Modern First-Principles View on Ligand Field Theory Through the Eyes of Correlated Multireference Wavefunctions. In *Molecular Electronic Structures of Transition Metal Complexes II*; Mingos, D. M. P., Day, P., Dahl, J. P., Eds.; Structure and Bonding, Vol. 143; Springer Berlin Heidelberg, 2012; pp 149–220. DOI: 10.1007/430_2011_57.

(38) Lin, C.-Y.; Guo, J.-D.; Fettinger, J. C.; Nagase, S.; Grandjean, F.; Long, G. J.; Chilton, N. F.; Power, P. P. Dispersion force stabilized two-coordinate transition metal-amido complexes of the -N(SiMe3)Dipp (Dipp = C6H3-2,6-Pr(i)2) ligand: structural, spectroscopic, magnetic, and computational studies. *Inorg. Chem.* **2013**, *52* (23), 13584–13593. DOI: 10.1021/ic402105m.

(39) Dolomanov, O. V.; Bourhis, L. J.; Gildea, R. J.; Howard, J.; Puschmann, H. OLEX2: a complete structure solution, refinement and analysis program. *J. Appl. Crystallogr.* **2009**, *42* (2), 339–341. DOI: 10.1107/S0021889808042726.

(40) Sheldrick, G. M. Crystal structure refinement with SHELXL. *Acta. Crystallogr. C* **2015**, *71* (Pt 1), 3–8. DOI: 10.1107/S2053229614024218.

(41) Farrugia, L. J. WinGX suite for small-molecule single-crystal crystallography. *J. Appl. Crystallogr.* **1999**, *32* (4), 837–838. DOI: 10.1107/S0021889899006020.

(42) Betteridge, P. W.; Carruthers, J. R.; Cooper, R. I.; Prout, K.; Watkin, D. J. CRYSTALS version 12: software for guided crystal structure analysis. *J. Appl. Crystallogr.* **2003**, *36* (6), 1487. DOI: 10.1107/S0021889803021800.

(43) *International tables for crystallography*, 1st online ed.; International Union of Crystallography; Springer, 2006.

(44) SADABS-2016/2. *Bruker*, 2016.

(45) X-Area, X.-R. 1. *STOE*, 2016.

(46) Kahn, O. *Molecular magnetism*; VCH, 1993.

(47) Roos, B. O.; Taylor, P. R.; Sigbahn, P. E. A complete active space SCF method (CASSCF) using a density matrix formulated super-CI approach. *Chem. Phys.* **1980**, *48* (2), 157–173. DOI: 10.1016/0301-0104(80)80045-0.

(48) Angeli, C.; Evangelisti, S.; Cimiraglia, R.; Maynau, D. A novel perturbation-based complete active space–self-consistent-field algorithm: Application to the direct calculation of localized orbitals. *J. Chem. Phys.* **2002**, *117* (23), 10525–10533. DOI: 10.1063/1.1521434.

(49) Angeli, C.; Cimiraglia, R.; Evangelisti, S.; Leininger, T.; Malrieu, J.-P. Introduction of n -electron valence states for multireference perturbation theory. *J. Chem. Phys.* **2001**, *114* (23), 10252–10264. DOI: 10.1063/1.1361246.

(50) Angeli, C.; Cimiraglia, R.; Malrieu, J.-P. N-electron valence state perturbation theory: a fast implementation of the strongly contracted variant. *Chem. Phys. Lett.* **2001**, *350* (3-4), 297–305. DOI: 10.1016/S0009-2614(01)01303-3.

(51) Neese, F. Efficient and accurate approximations to the molecular spin-orbit coupling operator and their use in molecular g-tensor calculations. *J. Chem. Phys.* **2005**, *122* (3), 34107. DOI: 10.1063/1.1829047.

(52) Ganyushin, D.; Neese, F. First-principles calculations of zero-field splitting parameters. *J. Chem. Phys.* **2006**, *125* (2), 24103. DOI: 10.1063/1.2213976.

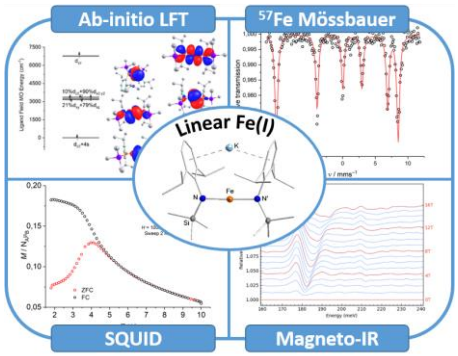
Ab-initio LFT
57Fe Mössbauer
Linear Fe(I)
SQUID
Magneto-IR